

Materials Science

Special Topic: Two-dimensional Materials and Devices

Halide vapor phase epitaxy of monolayer molybdenum diselenide single crystals

Taotao Li^{1,#,*}, Yang Yang^{1,#}, Liqi Zhou², Wenjie Sun², Weiyi Lin³, Lei Liu¹, Xilu Zou¹, Si Gao⁴, Yuefeng Nie², Yi Shi¹ & Xinran Wang^{1,5,6,*}¹National Laboratory of Solid State Microstructures, School of Electronic Science and Engineering and Collaborative Innovation Center of Advanced Microstructures, Nanjing University, Nanjing 210093, China;²National Laboratory of Solid State Microstructures, Jiangsu Key Laboratory of Artificial Functional Materials, College of Engineering and Applied Sciences and Collaborative Innovation Center of Advanced Microstructures, Nanjing University, Nanjing 210093, China;³School of Electronic Science and Engineering, Xiamen University, Xiamen 361005, China;⁴College of Material Science and Engineering, Nanjing Tech University, Nanjing 201110, China;⁵School of Integrated Circuits, Nanjing University, Suzhou 215163, China;⁶Suzhou Laboratory, Suzhou 215000, China

#Contributed equally to this work.

*Corresponding authors (emails: ttli@nju.edu.cn (Taotao Li); xrwan@nju.edu.cn (Xinran Wang))

Received 4 October 2022; Revised 7 December 2022; Accepted 29 December 2022; Published online 12 April 2023

Abstract: Single-crystalline transition metal dichalcogenides (TMD) films are of potential application in future electronics and optoelectronics. In this work, a halide vapor phase epitaxy (HVPE) strategy was proposed and demonstrated for the epitaxy of molybdenum diselenide (MoSe₂) single crystals, in which metal halide vapors were *in-situ* produced by the chlorination of molybdenum as sources for the TMD growth. Combined with the epitaxial sapphire substrate, unidirectional domain alignment was successfully achieved and monolayer single-crystal MoSe₂ films have been demonstrated on a 2-inch wafer for the first time. A series of characterizations ranging from centimeter to nanometer scales have been implemented to demonstrate the high quality and uniformity of the MoSe₂. This work provides a universal strategy for the growth of TMD single-crystal films.

Keywords: halide vapor phase epitaxy, single-crystal, molybdenum diselenide, 2D semiconductor, wafer-scale

INTRODUCTION

Transition metal dichalcogenides (TMDs) have atomic-limit layered structures, wide varieties, and the feasibility of van der Waals assembling, and possess great potential for future electronic and optoelectronic devices [1–5]. To become practically useful for electronics, large-scale single-crystalline TMD films need to be grown in controllable ways. In the past decade, the chemical vapor deposition (CVD) method has made huge progress in the growth of TMD films, and wafer-scale single-crystal MoS₂ and WS₂ films have been realized [6,7]. However, for selenide-based TMDs, only discrete flakes are always produced, while polycrystal films have been achieved by metal-organic CVD (MOCVD) [8,9] and molecular beam epitaxy

(MBE) [10]. The controllable growth of continuous single-crystal selenide TMD film remains a challenge.

Two requirements must be satisfied to grow a single-crystal TMD film: (1) a symmetry-matched single-crystal substrate that enables the unidirectional domain epitaxy [11–13]; (2) a growth process that enables stable, precise, and continuous vapor source flux, which ensures the domains' continuous growth and merging. For the substrate issue, some solutions have been successfully implemented such as single-crystal Au (111) [14–16], C/A sapphire [6], and A-plane sapphire [7]. On the other hand, the precise and stable flux control, which is a main disadvantage of the present CVD method compared with MOCVD and MBE, has been rarely discussed in the literature. Herein, the oxide powder precursors widely used in CVD growth are considered difficult to achieve precise control over the growth of the selenides due to the following reasons. (1) The vapor phase of metal oxide precursors consists predominantly of ringlike molecules such as $(\text{MoO}_3)_3$ and $(\text{WO}_3)_3$ [17,18], which suffer high energy barriers to break the ring and react with chalcogens [19,20]. For instance, the growth of MoS_2 by MoO_3 with S suffers a rate-limiting barrier of 0.95 eV to break the Mo_3 -containing chain [19,20]. This barrier should be much higher for Se since Se is less reductive than S. (2) The growth of selenides requires the assistance of H_2 to reduce the oxides [21] and protect the material from etching due to the avoidable air leaking in low-pressure growth. However, introducing H_2 in turn reduces the metal oxides to elemental metals and terminates the source volatilization. Therefore, selecting suitable precursors and designing reasonable control methods are the keys to the growth of continuous TMD films.

In this work, we propose a halide-vapor phase epitaxy (HVPE) strategy to realize the epitaxy of MoSe_2 single-crystal films. HVPE has been widely used in the semiconductor industry for the growth of GaN, Ga_2O_3 , etc. [22,23]. In contrast to metal oxides, halides are more volatile. For instance, the boiling point of MoCl_5 is 268°C (vapor pressure 10^5 Pa). At this temperature, the vapor pressure of MoO_3 is estimated to be 1.4×10^{-12} Pa according to the Clausius-Clapeyron equation for the vaporization of solid MoO_3 [24]. And importantly, the halide vapors can be feasibly obtained by the *in-situ* reaction of HCl gas with metals, which enables the stable supply and precise control of the metal sources. Here, we extend HVPE to the growth of TMDs and demonstrate wafer-scale single-crystal MoSe_2 film for the first time. Combined with the C/A sapphire substrate [6], unidirectional MoSe_2 domains and continuous single-crystal films have been achieved on a 2-inch wafer. Our result may represent a step forward to the large-scale fabrication of single-crystal TMD films in a controllable way, especially for refractory metals such as Mo, W, Nb, and Ta.

MATERIALS AND METHODS

Substrate design and annealing

Single-side polished sapphire (0001) substrates with a designed miscut angle of 1° toward the A-axis (denoted as C/A- 1°) were purchased from HeFei crystal Technical Material Co., Ltd. and Aurora Optoelectronics Co., Ltd. Before growth, the substrates were annealed at 1000 – 1200°C for 4 h in the air, which produces uniformly distributed M-direction bi-steps with about 0.43 nm in height.

Growth process

This experiment was carried out in a three-temperature zone tube furnace with a diameter of 60 mm. The

system was schematically shown in Figure S1. Mo metal flake (99.99% in purity, $\sim 2 \text{ cm}^2$ in area) and Se powder (60 g) were used as source materials. The Se powder was placed in a quartz crucible and heated to 280–300°C using an additional heating mantle. The carrier gas for the Se source was 100 sccm Ar + 20 sccm H_2 (sccm = standard cubic centimeter per minute). H_2 plays a vital role in MoSe_2 growth that keeps a reducing atmosphere during the deposition process. The flux of Se vapor was estimated to be about 100–120 mg/min to keep a Se-rich condition. The Mo metal flake was placed in a small tube separate from the Se vapor and heated in the heating zone I of the furnace at 700°C. The carrier gas for Mo metal was Ar + HCl, which produces volatile MoCl_x gas for MoSe_2 growth. For the supply of HCl gas, NH_4Cl (2 g) powders or HCl/Ar mixture (10 vol% HCl) were used. The NH_4Cl powders were placed in a container outside of the growth chamber connecting to the Mo tube and heated to 320–340°C with an independent heating mantle to *in-situ* release HCl gas. The flux of NH_4Cl was estimated to be about 5 mg/min (equivalent to ~ 2 sccm HCl vapor). For better control, the HCl/Ar mixture (10 vol% HCl) with a flow of 20 sccm was controlled by the mass flow controller.

For the growth, the substrate was heated firstly with a ramping up speed of 30°C/min to 1000°C, and then followed by the heating of Mo foil and Se source. During the ramping stage, 100 and 50 sccm Ar passed through Se and Mo, respectively. When the substrate and sources reached the setting temperatures (until Se melted totally), H_2 for Se and HCl for Mo were switched on and growth began. The growth pressure was about 1.5 mbar (1 bar = 10^5 Pa). The growth of unidirectional domains and continuous films takes 10 and 30 min, respectively.

After growth was complete, turn off HCl or stop heating NH_4Cl . The heating of Se powder and H_2 was kept till the sample cooled to 300°C to avoid the decomposition of the as-grown MoSe_2 .

Transfer of TEM samples

The TEM sample is prepared by a PMMA-assisted method. First, a PMMA thin film was spin-coated on the top of the MoSe_2 /sapphire substrate. Then, the sample was immersed in 2 mol/L KOH solution and the PMMA/ MoSe_2 layer would lift off. The PMMA/ MoSe_2 was then transferred onto the TEM grid (GIG-1010-3C) and heated at 120°C for 1 min to strengthen the adhesion among PMMA/ MoSe_2 /Grid. Finally, PMMA was subsequently washed off with acetone.

Characterization

Raman and photoluminescence (PL) spectra were excited by a homemade system with 488-nm laser excitation and the Princeton instrument SP-2500 spectrometer. Atomic force microscope (AFM) testing was performed by the Asylum Cypher S system. Second-harmonic generation (SHG) mapping was collected in a photon counter (HAMAMATSU H7421-50) and 1550-nm laser (Rainbow1550-Dichro). Reflection high-energy electron diffraction (RHEED, STAIB Instruments) and low-energy electron diffraction (LEED, OCI, BDL600IR-MCP) were measured at room temperature under the ultrahigh vacuum of 10^{-9} and 10^{-10} Torr, respectively. The electron acceleration voltage was 15 kV for RHEED and 190 V for LEED. The probe diameter was 1 mm for LEED. High-angle annular dark field scanning transmission electron microscopy (HAADF-STEM) was performed on an aberration-corrected STEM Titan Cubed G2 60-300 system with an

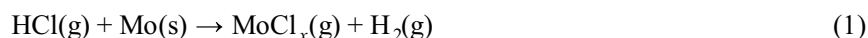
accelerating voltage of 60 and 300 kV respectively for MoSe₂ layers and cross-sectional MoSe₂/sapphire HAADF-STEM.

RESULTS

HVPE strategy for MoSe₂

The continuous and stable supply of source gases is a key to growing continuous TMD films. Figure 1 proposes a general strategy for the HVPE synthesis of TMDs. Taking MoSe₂ for instance, metallic molybdenum foils were heated at elevated temperatures and reacted with HCl vapors, *in-situ* producing MoCl_x vapors. Thus, a precisely fixed flow of HCl vapor going through the heating Mo foil *in-situ* releases MoCl_x vapors with controlled flux, which enables the continued growth of MoSe₂ in a controllable way, as shown in the schematic in Figure 1 and Equations (1)–(3).

The main reactions may include:



Unidirectional epitaxy of MoSe₂ domains

In addition to the HVPE process, a symmetry-matched substrate is also required to realize the unidirectional alignment of two-dimensional (2D) domains to achieve large-area single crystals. In the previous work, we utilized a C/A-1° sapphire substrate and successfully realized single-crystal MoS₂ growth [6]. Here, the same substrates were used, and the unidirectional growth of MoSe₂ was realized by utilizing the HVPE process, as shown in the schematic in Figure 2A. The optical micrograph of MoSe₂ domains grown on C/A sapphire was shown in Figure 2B and Figure S2. It can be seen that the triangular domains are aligned unidirectionally on the substrate surface. These grain sizes are approximately 10–25 μm. The AFM characterization shows a clean and smooth surface without contamination, wrinkles, or particles, which is important for future device applications. The thickness is 0.7 nm, confirming the monolayer MoSe₂ (Figure 2C). The triangular grains were further confirmed by Raman spectroscopy (Figure 2D) and PL spectroscopy (Figure 2E). In the Raman spectrum, two peaks at 240.5 and 287.8 cm⁻¹ were observed, corresponding to the two characteristic peaks A_{1g} and E_{2g}¹ of MoSe₂, respectively. The PL spectrum shows a strong peak at 1.57 eV, following the direct

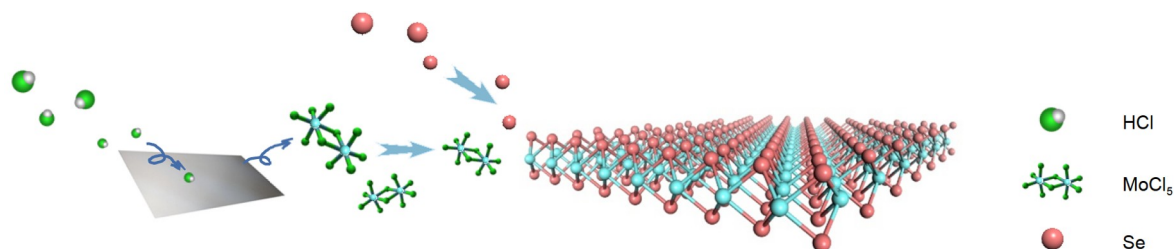


Figure 1 A schematic for the HVPE synthesis of MoSe₂.

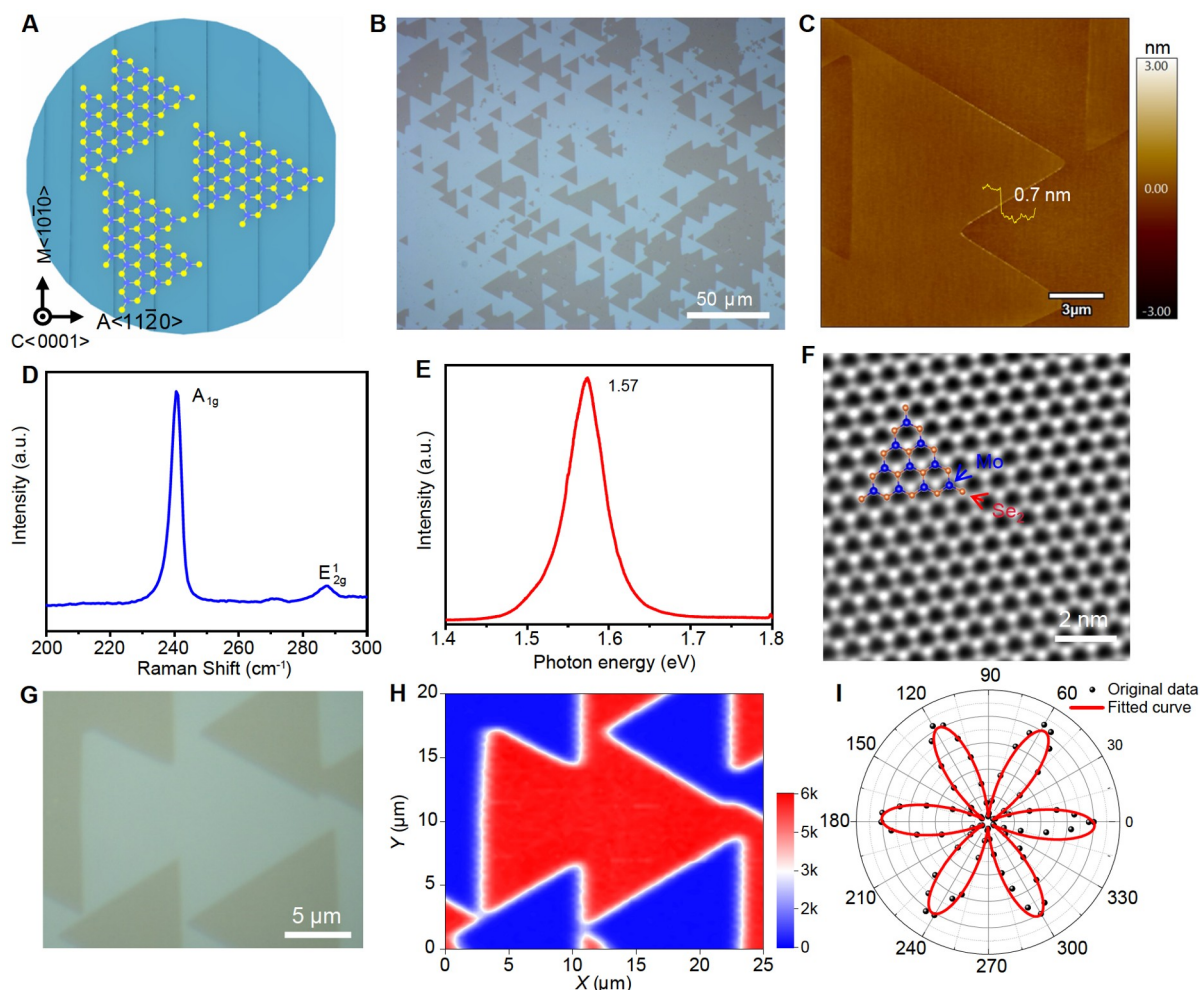


Figure 2 Unidirectional epitaxy of MoSe₂ domains on C/A-1° sapphire substrate. (A) Schematic of the unidirectional alignment of MoSe₂ domains on the C/A sapphire with the domain edge parallel to the M-steps. (B) Optical microscopy image of unidirectional MoSe₂ domains. (C) AFM image of MoSe₂ domains showing the high surface cleanliness and the relationship between the domain edge and surface steps. (D, E) Raman and PL spectrum of the as-grown MoSe₂. (F) Atomic-resolution HAADF-STEM image of MoSe₂ basal plane. (G, H) Polarized SHG mapping of merging MoSe₂ domains and corresponding optical image. (I) Polar plot of the SHG intensity and theoretical fitting revealing the Zig-Zag edge of the triangle MoSe₂ domains.

band-gap of monolayer MoSe₂. For atomic-scale characterization, the domains were transferred and further characterized by a scanning transmission electron microscope (STEM), as shown in Figure 2F. These atomic arrangements show a perfect hexagonal structure, where the brighter spots correspond to the stacked Se₂ atoms and the darker spots correspond to the Mo atoms [25].

It is noted that the unidirectional alignment of domains is the key to achieving an entire single-crystal TMD film, which enables the perfect atomic merging between domains, as previously reported [6,14]. Here we confirm that situation applies to the case of MoSe₂. Polarized second harmonic generation (SHG) is a fast, efficient, and damage-free method for characterizing grain boundaries [26]. Figures 2G and 2H show the optical microscopy and corresponding SHG mapping images showing several merging unidirectional domains. It can be observed that the SHG intensity is uniform within and across the domains, indicating no grain boundaries at the domain junctions [6,26]. In addition, the polarized SHG intensity plot of the triangular

MoSe₂ recognized that the triangular MoSe₂ domain has Zig-Zag [11 $\bar{2}$ 0] edges, along which the SHG signal is minimal (Figures 2H and 2I). Combined with the AFM results shown in Figure 2C, it is worth noting that the Zig-Zag [11 $\bar{2}$ 0] edges of the triangle parallel the M-steps of the C/A sapphire, indicating a 30° rotation of crystal relative to that of sapphire [6], which was the basis of the unidirectional alignment and would be discussed later.

Wafer-scale single-crystal MoSe₂ film

By extending the growth time, wafer-scale MoSe₂ single crystals on 2-inch C/A sapphire can be obtained

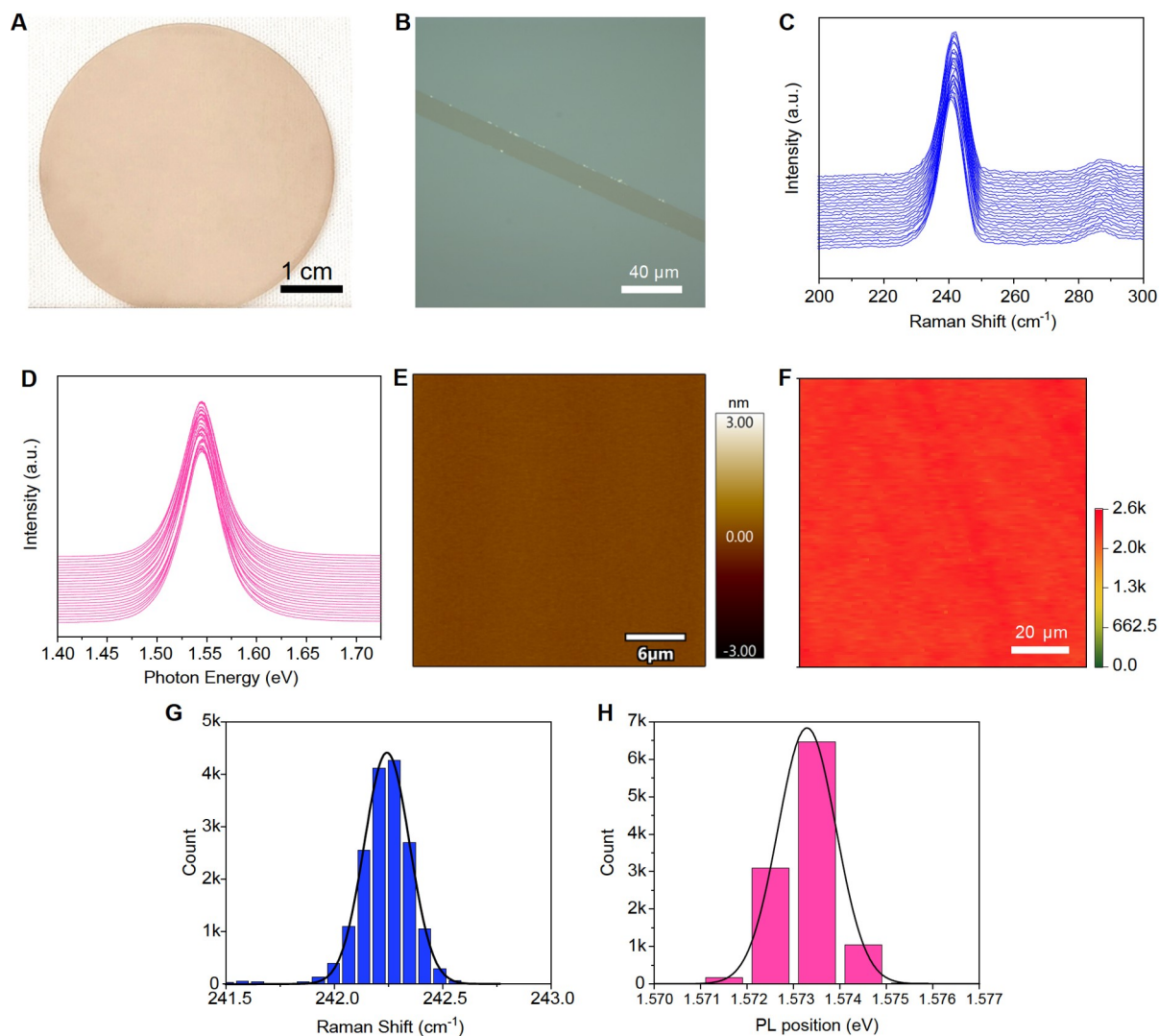


Figure 3 Wafer-scale MoSe₂ single crystals. (A) Photograph of 2-inch monolayer MoSe₂ single-crystal film on C/A-1° sapphire substrate. (B) Optical microscopy image showing the cleanliness, uniformity, and continuity of the as-grown MoSe₂ film. A scratch was made for the optical contrast. (C, D) Raman and PL line scans across a 2-inch MoSe₂ single-crystal film. (E) AFM height image of as-grown MoSe₂ film, displaying a clean and wrinkle-free surface. (F) SHG mapping over 100 μm×100 μm, revealing the single-crystal feature of the as-grown MoSe₂ film. (G, H) Statistical distributions of the Raman and PL peak position from three mapping zones (16875 Raman spectra, 10800 PL spectra).

(Figure 3A). Optical microscopy image shows a clean and uniform surface (Figure 3B). Raman and PL line scans across a 2-inch MoSe₂ wafer (25 spectra with 2-mm step) show no obvious variations in peak position and linewidth (Figures 3C and 3D). We further performed high-resolution PL and Raman mapping in several areas on the same wafer (Figures S3 and S4). Statistical analysis of 10800 PL spectra from three different mapping zones reveals an average PL position of 1.573 eV with a standard deviation of 0.6 meV (Figure 3H), and FWHM ranging from 53.4–59.4 meV (Figure S3). Raman data collected from 16875 spectra demonstrated a Raman shift averaged at 242.20 cm⁻¹ with a standard deviation of 0.12 cm⁻¹ (Figure 3G), and FWHM of 6.6–7.2 cm⁻¹ (Figure S4). AFM image showed uniform and wrinkle-free monolayer MoSe₂ film with low roughness of 50 pm (Figure 3E).

To further confirm the single-crystalline nature of the MoSe₂ films, SHG mapping, LEED, dark-field TEM (DF-TEM), and HAADF-STEM were performed. As shown in Figure 3F, the SHG mapping on continuous films shows uniform signal intensity without any evidence of poly-crystallinity and grain boundaries. In contrast, for the poly-crystal MoSe₂ films grown on C/M sapphire, grain boundaries were observed in SHG mapping (Figure S5). Figure S6 shows LEED patterns measured at 9 different locations across a 1-cm² sample cut from a wafer. The patterns showed three bright spots at certain voltages, as expected for C₃ symmetry, unambiguously proving the single-crystalline feature of MoSe₂ film. In addition, DF-TEM characterization of fully coalesced MoSe₂ films was performed in a scan over 2 mm, confirming its single-crystalline nature (Figure S7). For the atomic-scale investigation, HAADF-STEM was performed for the continuous film. The data collected from multiple locations show identical lattice orientation without obvious rotation or inversion, indicating no tilt or twin grain boundaries (Figure S8) [6]. In addition, a H₂O vapor etching process was performed on the as-grown MoSe₂ [27] and no grain boundaries were found (Figure S9). These results prove that our MoSe₂ films have excellent uniformity from the sub-micrometer to the centimeter scale.

Epitaxial relationship and mechanism

Next, the epitaxial relationship of MoSe₂ on the sapphire surface, as well as the role of surface steps should be discussed. We use RHEED and cross-sectional HAADF-STEM to reveal the epitaxial relationship between MoSe₂ and c-sapphire. Figures 4A and 4B show the RHEED results of the electron beam along the M-axis and A-axis of sapphire, i.e., the $\langle 10\bar{1}0 \rangle$ and $\langle 11\bar{2}0 \rangle$ direction, respectively. The diffraction information from the sapphire substrate and MoSe₂ were distinguished. The spot-like diffraction (denoted by white arrows) comes from the sapphire substrate, while the strip-like diffraction fringes (marked by red arrows) come from MoSe₂. The diffraction fringes of both crystals are equidistantly distributed and no unequally spaced diffraction bands were observed, indicating that MoSe₂ grains align without other orientations. In addition, we calculated the ratio of the diffraction pattern spacing between the substrate and MoSe₂, from both M- and A-directions of sapphire, which was calculated to be 1.2 and 2.5, respectively. According to the lattice constants of MoSe₂ and sapphire, it can be inferred that $\sqrt{3} a_{(\text{MoSe}_2)} / a_{(\text{Al}_2\text{O}_3)} = 1.2$ and $\sqrt{3} a_{(\text{Al}_2\text{O}_3)} / a_{(\text{MoSe}_2)} = 2.5$, where $a_{(\text{sapphire})} = 4.76 \text{ \AA}$, $a_{(\text{MoSe}_2)} = 3.29 \text{ \AA}$. That is to say, there is an included angle of 30° between the MoSe₂ lattice vector and the sapphire lattice vector. In addition, the STEM characterization of the cross-section of the sample was also performed. On the M-plane of sapphire, the lattice period of MoSe₂ is 0.285 nm ($\sqrt{3} a_{(\text{MoSe}_2)} / 2 = 0.285 \text{ nm}$), and that of sapphire is 0.238 ($a_{(\text{Al}_2\text{O}_3)} / 2 = 0.238 \text{ nm}$), as shown in Figure 4C and

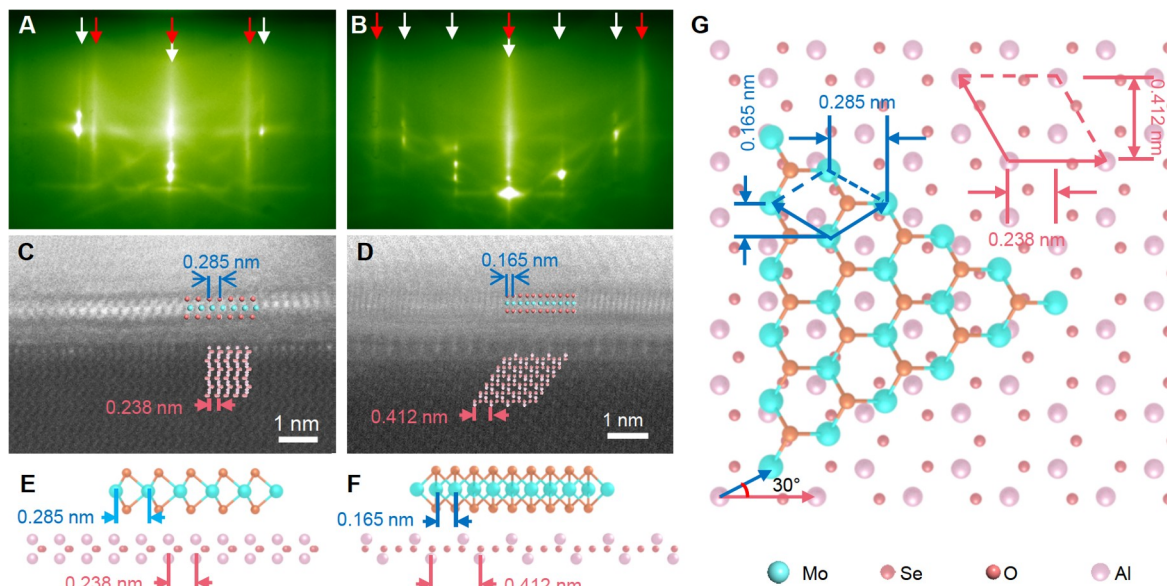


Figure 4 Epitaxial relationship between MoSe₂ and C-sapphire. (A, B) RHEED pattern of MoSe₂/sapphire along Al₂O₃ <10 $\bar{1}$ 0> and <11 $\bar{2}$ 0> directions, respectively. The white and red arrows denote diffraction patterns from sapphire and MoSe₂, respectively. (C, D) Cross-sectional HAADF-STEM images of the as-grown MoSe₂/Al₂O₃ interface along Al₂O₃ <10 $\bar{1}$ 0> and <11 $\bar{2}$ 0> directions, respectively. (E, F) Schematic of the atomic arrangement along Al₂O₃ <10 $\bar{1}$ 0> and <11 $\bar{2}$ 0> directions, respectively. (G) The epitaxial relationship of MoSe₂ on sapphire (0001) substrate. Red and blue arrows indicate the lattice vectors of sapphire and MoSe₂.

schematized in Figure 4E. On the A-plane of sapphire, the lattice period of MoSe₂ is 0.165 nm ($a_{\text{MoSe}_2}/2 = 0.165$ nm), and that of sapphire is 0.412 ($\sqrt{3} a_{\text{Al}_2\text{O}_3}/2 = 0.412$ nm), as shown in Figures 4D and 4F. The results of cross-sectional HAADF-STEM perfectly match with that of RHEED, unambiguously proving the R30° relationship between MoSe₂ and sapphire (0001), as shown in Figure 4G. This is consistent with the epitaxial relationship of MoS₂ on sapphire [6]. It is also observed that a less ordered layer exists at the MoSe₂/sapphire interface in the cross-section STEM images, indicating chalcogen passivation of sapphire for TMD epitaxy, which has been previously reported [9,28].

Based on the R30° relationship, we can infer that MoSe₂ <11 $\bar{2}$ 0> // Al₂O₃ <10 $\bar{1}$ 0>, i.e., the Zig-Zag edge of MoSe₂ parallels the M-steps of sapphire. Therefore, in the initial nucleation stage, the M-steps facilitate the nucleation and break the formation energy degeneracy. Combined with the van der Waals interactions, only one direction favors the nucleation and forms the unidirectional domain alignment, just as in the case of MoS₂ on sapphire [6].

DISCUSSION

The TMD family contains a large member of materials with similar crystal structures, which follow approximative epitaxial behavior on the substrate. However, their distinct chemical properties make the growth processes differ from each other. In this work, we demonstrated an HVPE strategy for the epitaxy of MoSe₂ single crystal, where the metal halide vapors were *in-situ* produced and contributed to the controllable growth of MoSe₂ films. Due to the similar R30° epitaxial behavior to that of MoS₂ on sapphire as previously reported

[6], a custom-designed C/A-1° sapphire substrate with M-steps was used, realizing a unidirectional domain alignment and subsequent stitching into 2-inch single-crystal wafer. The HVPE method guarantees stable and precise source flux and enables the controllable growth of a continuous monolayer MoSe₂ single-crystal film. This strategy may pave the way to the universal epitaxy of single-crystal TMD films.

Data availability

The original data are available from corresponding authors upon reasonable request.

Funding

This work was supported by the National Key R&D Program of China (2022YFB4400100 and 2021YFA0715600), the Leading-edge Technology Program of Jiangsu Natural Science Foundation (BK20202005), the National Natural Science Foundation of China (T2221003, 61927808, 61734003, 61861166001, and 62204113), the Natural Science Foundation of Jiangsu Province (BK20220773), the Strategic Priority Research Program of Chinese Academy of Sciences (XDB30000000), and Key Laboratory of Advanced Photonic and Electronic Materials, Collaborative Innovation Center of Solid-State Lighting and Energy-Saving Electronics, and the Fundamental Research Funds for the Central Universities, China.

Author contributions

X.W. and T.L. conceived and supervised the project. T.L. and Y.Y. designed the research and analyzed the data. Y.Y. performed the CVD growth with assistance from T.L., L.L., and X.Z. Y.Y. and W.L. collected and analyzed the PL, Raman, and SHG data. W.S. and Y.N. performed the RHEED and LEED characterization and data analysis. L.Z. and S.G. performed the TEM characterization and data analysis. T.L., Y.Y., and X.W. co-wrote the manuscript with input from other authors. All authors contributed to discussions.

Conflict of interest

The authors declare no conflict of interest.

Supplementary information

The supporting information is available online at <https://doi.org/10.1360/nso/20220055>. The supporting materials are published as submitted, without typesetting or editing. The responsibility for scientific accuracy and content remains entirely with the authors.

References

- 1 Zhou J, Lin J, Huang X, *et al.* A library of atomically thin metal chalcogenides. *Nature* 2018; **556**: 355–359.
- 2 Kang K, Lee KH, Han Y, *et al.* Layer-by-layer assembly of two-dimensional materials into wafer-scale heterostructures. *Nature* 2017; **550**: 229–233.
- 3 Zhu K, Wen C, Aljarb AA, *et al.* The development of integrated circuits based on two-dimensional materials. *Nat Electron* 2021; **4**: 775–785.
- 4 Withers F, Del Pozo-Zamudio O, Mishchenko A, *et al.* Light-emitting diodes by band-structure engineering in van der Waals heterostructures. *Nat Mater* 2015; **14**: 301–306.
- 5 Tang H, Zhang H, Chen X, *et al.* Recent progress in devices and circuits based on wafer-scale transition metal dichalcogenides. *Sci China Inf Sci* 2019; **62**: 220401.
- 6 Li T, Guo W, Ma L, *et al.* Epitaxial growth of wafer-scale molybdenum disulfide semiconductor single crystals on sapphire. *Nat Nanotechnol* 2021; **16**: 1201–1207.

- 7 Wang J, Xu X, Cheng T, *et al.* Dual-coupling-guided epitaxial growth of wafer-scale single-crystal WS₂ monolayer on vicinal a-plane sapphire. *Nat Nanotechnol* 2022; **17**: 33–38.
- 8 Zhang X, Choudhury TH, Chubarov M, *et al.* Diffusion-controlled epitaxy of large area coalesced WSe₂ monolayers on sapphire. *Nano Lett* 2018; **18**: 1049–1056.
- 9 Lin YC, Jariwala B, Bersch BM, *et al.* Realizing large-scale, electronic-grade two-dimensional semiconductors. *ACS Nano* 2018; **12**: 965–975.
- 10 Poh SM, Zhao X, Tan SJR, *et al.* Molecular beam epitaxy of highly crystalline MoSe₂ on hexagonal boron nitride. *ACS Nano* 2018; **12**: 7562–7570.
- 11 Dong J, Zhang L, Dai X, *et al.* The epitaxy of 2D materials growth. *Nat Commun*, 2020, **11**: 5862.
- 12 Bets KV, Gupta N, Yakobson BI. How the complementarity at vicinal steps enables growth of 2D monocrystals. *Nano Lett* 2019; **19**: 2027–2031.
- 13 Chubarov M, Choudhury TH, Hickey DR, *et al.* Wafer-scale epitaxial growth of unidirectional WS₂ monolayers on sapphire. *ACS Nano* 2021; **15**: 2532–2541.
- 14 Yang P, Zhang S, Pan S, *et al.* Epitaxial growth of centimeter-scale single-crystal MoS₂ monolayer on Au(111). *ACS Nano* 2020; **14**: 5036–5045.
- 15 Li J, Wang S, Jiang Q, *et al.* Single-crystal MoS₂ monolayer wafer grown on Au(111) film substrates. *Small* 2021; **17**: 2100743.
- 16 Choi SH, Kim HJ, Song B, *et al.* Epitaxial single-crystal growth of transition metal dichalcogenide monolayers via the atomic sawtooth Au surface. *Adv Mater* 2021; **33**: 2006601.
- 17 Berkowitz J, Inghram MG, Chupka WA. Polymeric gaseous species in the sublimation of molybdenum trioxide. *J Chem Phys* 1957; **26**: 842–846.
- 18 Berkowitz J, Chupka WA, Inghram MG. Polymeric gaseous species in the sublimation of tungsten trioxide. *J Chem Phys* 1957; **27**: 85–86.
- 19 Lei J, Xie Y, Yakobson BI. Gas-phase “prehistory” and molecular precursors in monolayer metal dichalcogenides synthesis: The case of MoS₂. *ACS Nano* 2021; **15**: 10525–10531.
- 20 Lei J, Xie Y, Kutana A, *et al.* Salt-assisted MoS₂ growth: Molecular mechanisms from the first principles. *J Am Chem Soc* 2022; **144**: 7497–7503.
- 21 Liu B, Fathi M, Chen L, *et al.* Chemical vapor deposition growth of monolayer WSe₂ with tunable device characteristics and growth mechanism study. *ACS Nano* 2015; **9**: 6119–6127.
- 22 Hu J, Wei H, Yang S, *et al.* Hydride vapor phase epitaxy for gallium nitride substrate. *J Semicond* 2019; **40**: 101801.
- 23 Xiu X, Zhang L, Li Y, *et al.* Application of halide vapor phase epitaxy for the growth of ultra-wide band gap Ga₂O₃. *J Semicond* 2019; **40**: 011805.
- 24 Gulbransen EA, Andrew KF, Brassart FA. Vapor pressure of molybdenum trioxide. *J Electrochem Soc* 1963; **110**: 242–243.
- 25 Chen J, Zhao X, Tan SJR, *et al.* Chemical vapor deposition of large-size monolayer MoSe₂ crystals on molten glass. *J Am Chem Soc* 2017; **139**: 1073–1076.
- 26 Yin X, Ye Z, Chenet DA, *et al.* Edge nonlinear optics on a MoS₂ atomic monolayer. *Science* 2014; **344**: 488–490.
- 27 Wang J, Xu X, Qiao R, *et al.* Visualizing grain boundaries in monolayer MoSe₂ using mild H₂O vapor etching. *Nano Res* 2018; **11**: 4082–4089.
- 28 Xiang Y, Sun X, Valdman L, *et al.* Monolayer MoS₂ on sapphire: An azimuthal reflection high-energy electron diffraction perspective. *2D Mater* 2020; **8**: 025003.